American Mineralogist, Volume 89, pages 1033–1042, 2004

Dehydration and rehydration process in boggsite: An in situ X-ray single-crystal study

STEFANO ZANARDI,[1,*] GIUSEPPE CRUCIANI,[1] ALBERTO ALBERTI,[1] AND ERMANNO GALLI[2]

[1]Dipartimento di Scienze della Terra, Università di Ferrara, Corso Ercole I° d'Este, 32, I-44100 Ferrara, Italy
[2]Dipartimento di Scienze della Terra, Università di Modena e Reggio Emilia, Largo S. Eufemia, 19, I-41100 Modena, Italy

ABSTRACT

The dehydration-rehydration process in boggsite $|K_{0.06}Na_{0.36}Sr_{0.01}Ca_{7.00}Mg_{1.20}Fe_{0.05}(H_2O)_{70}|[Al_{17.52}Si_{78.62}O_{192}]$-**BOG**, a rare natural pentasil zeolite characterized by a 3D channel system of 10- and 12-rings, occurs in space group *Imma* with cell parameters $a = 20.291(1)$, $b = 23.840(1)$, $c = 12.807(1)$ Å, and $V = 6195.2$ Å^3 at 25 °C. Single-crystal X-ray data collections were carried out at room temperature, at 150, 350, and 500 °C in a hot nitrogen stream, and after the crystal was cooled down to 150 °C and then again at room temperature. During these processes, the variation in the unit-cell volume was always less than 1.4%. At room conditions boggsite is characterized by strong disorder in cation and H_2O molecule distribution, with many partially occupied sites weakly interacting with the framework. At 150 °C, where most of the water is lost, three extraframework cation sites were located. At 350 °C boggsite is fully dehydrated and five cation sites are present; three of these are fourfold coordinated and the others are sixfold coordinated. As a consequence of the migration of the cations, at 500 °C only four cation sites are present. The rehydration process causes distortion of the boggsite channels; the 10-ring reduces its free area by about 1 Å^2, whereas the area of the 12-ring channel grows from 40 to 42 Å^2. The dehydration process is rapid and completely reversible.

INTRODUCTION

Boggsite (IZA code **BOG,** Baerlocher et al. 2001) is a very rare zeolite discovered in Eocene basalts near Goble (Columbia County, Oregon) and first described by Howard et al. (1990). A second occurrence of this mineral was described by Galli et al. (1995) from the Jurassic Ferrar dolerites of Mt. Adamson (Northern Victoria Land, Antarctica). Both these studies reported a high Ca content in boggsite (~7 and ~5 Ca apfu in the Goble and Mt. Adamson samples, respectively). The crystal structure of boggsite, solved by Pluth and Smith (1990) with a sample from Goble, is characterized by a pentasil framework and an interesting 3D channel system of 10- and 12-rings. This topology has no counterpart among synthetic zeolites.

It is well known that one of the most remarkable properties of zeolites is their thermal behavior (i.e., stability, phase transformation, and rate and temperature of dehydration and rehydration); however, no investigations have been reported on the thermal stability of boggsite. In particular, considering the high Ca content of this zeolite and the often-reported evidence of low thermal stability of Ca-rich zeolites, which usually show a collapsed framework upon dehydration, it appears of interest to verify the possible occurrence of a collapsed phase in dehydrated boggsite. It is common knowledge that such structural modifications play an important role in assessing the suitability of a zeolite structure for technological applications (e.g., catalysis and molecular sieving). In fact, the accessibility and connectivity of the zeolite channel system is strongly reduced after framework collapse. The aim of this work is to study dehydration-rehydration processes in boggsite from room conditions to 500 °C by single-crystal X-ray diffraction.

* E-mail: zrs@unife.it

EXPERIMENTAL PROCEDURE AND REFINEMENT

The availability of relatively large, untwinned boggsite crystals from Mt. Adamson allowed us to perform an in situ single-crystal diffraction study. A single crystal of boggsite, measuring $0.17 \times 0.15 \times 0.20$ mm, was selected and glued to a quartz capillary with a very small amount of refractory cement (M-BOND GA-100) composed mainly of silica. This capillary was in turn inserted into an ENRAF NONIUS FR 559 goniometer head, made up according to the design proposed by Tuinstra and Fraase Storm (1978). The heater uses the principle of double gas streams flowing parallel to the goniometer head axis, which provide a cylindrical cool-gas stream that coaxially encloses the hot-gas jet. The crystal was heated by a hot nitrogen flow, and the temperature was measured with a thermocouple placed about 4 mm below the capillary.

Single-crystal data collections were performed with a Nonius four-circle diffractometer equipped with a CCD detector and Mo$K\alpha$ radiation. Seven data collections were carried out at the following temperatures: room temperature (BOG-RT), 150 °C (BOG-150), 350 °C (BOG-350), 500 °C (BOG-500), after cooling to 150 °C (BOG-150-R), and after cooling to room temperature (BOG-RT-R). To ensure that the sample reached a status as close as possible to its thermodynamic equilibrium and to prevent crystallinity loss, the heating profile was as follows: ramp from room temperature to 150 °C with a 2 °C/min heating rate, hold at 150 °C for about 14h prior to data collection, and then repeat this process up to 350 and 500 °C. A similar approach was followed for the cooling process from 500 to 150 °C and from 150 °C to RT, using a 3 °C/min cooling rate. To promote the rehydration of boggsite at room temperature, the sample was kept at this temperature for two days prior to data collection. Experimental details of the data collections are reported in Table 1. More details concerning the data collection parameters are given in Table 2. It should be noted that two data collections were performed at room temperature, the first using a standard goniometer, with better statistics and higher resolution (2θ up to 65°), and the second using the high-temperature goniometer head and the data collection parameters reported in Tables 1 and 2. For the sake of homogeneity we shall discuss the values obtained in the second data collection; the parameters obtained with the high-resolution data collection are available as deposit items.

The DENZO-SMN (Otwinowski and Minor 1997) package was used for refinement of the unit-cell parameters and data reduction. The SHELXL-93 (Sheldrick 1993) program was employed for all the crystal structure refinements. Systematic extinctions were always consistent with the orthorhombic topological symmetry *Imma*; the starting parameters used for refinement were taken from Pluth and Smith (1990). The extraframework cation sites were assigned on the basis of the electron

TABLE 1. Crystal structure refinement parameters

Composition	$\|K_{0.06}Na_{0.36}Sr_{0.01}Ca_{7.00}Mg_{1.20}Fe_{0.05}(H_2O)_{70}\|$ $[Al_{17.52}Si_{78.62}O_{192}]$					
Crystal size (mm)	$0.17 \times 0.15 \times 0.20$					
Sample name	BOG-RT	BOG-150	BOG-350	BOG-500	BOG-150-R	BOG-RT-R
Temperature	25 °C	150 °C	350 °C	500 °C	150 °C	25 °C
a (Å)	20.291(1)	20.099(1)	20.053(1)	20.041(1)	20.087(1)	20.295(1)
b (Å)	23.840(1)	23.746(1)	23.838(1)	23.814(1)	23.800(1)	23.843(1)
c (Å)	12.807(1)	12.814(1)	12.850(1)	12.869(1)	12.805(1)	12.802(1)
V (Å^3)	6195.2	6115.7	6142.6	6141.8	6121.7	6194.8
Space group	*Imma*	*Imma*	*Imma*	*Imma*	*Imma*	*Imma*
Maximum 2θ	50.1°	50.1°	50.1°	50.1°	50.1°	50.1°
Measured reflections	8771	9523	10002	10190	9962	7084
Unique reflections	2768	2785	2797	2808	2823	2425
Observed reflection > 3σ	2127	2037	1974	1945	2029	2032
R_{int}(%)	4.5	5.2	5.5	5.9	5.3	4.5
R1(%)	7.9	5.7	6.2	5.7	5.8	8.7
wR2(%)	22.5	14.9	16.1	13.1	15.8	23.4
GooF	1.07	1.10	1.05	1.12	1.06	1.12
No. of parameters	254	229	219	214	229	254
Largest diffraction peak and hole	1.33/–0.66 e/Å^3	0.51/–0.3 e/Å^3	0.67/–0.31 e/Å^3	0.32/–0.31 e/Å^3	0.59/–0.29 e/Å^3	1.31/–0.69 e/Å^3

TABLE 2. Data collection and cell determination parameters

Sample	BOG-RT	BOG-150	BOG-350	BOG-500	BOG-150-R	BOG-RT-R
No. of images:						
Cell determination	10 phi	10 phi	10 phi	10 phi	10 phi	10 phi
Data collection	90 phi	90 phi	90 phi	90 phi	90 phi	90 phi
	39 omega	39 omega	27 omega	27 omega	39 omega	39 omega
Exposure time:						
Cell determination	60 sec	60 sec	60 sec	60 sec	60 sec	60 sec
Data collection	200 sec	200 sec	200 sec	200 sec	200 sec	200 sec
Total rotation width	180° phi	180° phi	180° phi	180° phi	180° phi	180° phi
	78° omega	78° omega	54° omega	54° omega	54° omega	78° omega

densities localized in the Fourier maps. Crystallographic R1 (F_o based) factors for these structures, over the studied temperature range, varied between 8.7 and 5.7% (see Table 1). The highest R factors were obtained for the room-temperature refinements, where (as explained later) the electron density showed a number of disordered sites with low occupancies. Table 3 reports the atomic coordinates, occupancy, and temperature factors, Table 4 the T-O distances, Table 5 the T-O-T angles, and Table 6 the coordination distances of the extraframework cations.

The chemical composition of the crystal used for the data collection was obtained with an ARL-SEMQ microprobe in wavelength-dispersive mode operating at 15 kV, 10 mA, and using a beam size of 45 μm. A defocused beam and low beam count were chosen to minimize the Na loss. Seven point analyses were performed; their low variability indicated good compositional homogeneity of the crystal. The estimated H_2O value was taken from the value (17 wt%) given by Howard et al. (1990) for boggsite from Goble. Note the almost complete absence of sodium in this crystal, in contrast with the Na content found in other crystals from the same locality (Galli et al. 1995).

RESULTS

The framework of boggsite can be easily described by using two different sets of tetrahedra: the first is the Em sheet described by Alberti (1979), the second the **pp** chain of Smith (2000). The Em sheet, orthogonal to the [010] direction, is obtained by interconnecting chains of edge-sharing 4^25^4 units found in heulandite-group zeolites [f_2 chains in the notation of Alberti (1979)], which develop along [001]. The **pp** chain, which develops in the [100] direction, is obtained by alternating straight and zigzag four-rings of tetrahedra. These sets of tetrahedra alternate along [010], and are connected through O atom bridges forming 5^46^2 cages [**eun** polyhedral subunits according to Pluth and Smith (1990)]. In this way the four-connected 3D framework of boggsite is generated.

BOG-RT crystal structure

Framework. Six symmetrically independent tetrahedral sites are present in the boggsite framework. The (Si,Al) distribution for boggsite from Mt. Adamson was calculated according to the method of Alberti and Gottardi (1988), using the Si-O and Al-O distances given by the relationship reported in Alberti et al. (1990); this relationship incorporates parameters that account for the effects of framework and extraframework cations, along with those of the T-O-T and O-T-O angles. The results indicated partial Si/Al ordering, with Al distributed among the first four tetrahedral sites, and absent in T5 and T6. However, the overall Al content (13%) was far lower than that found in the chemical analysis (~17.5%). This discrepancy, which may be easily attributed to the very large temperature factor of the framework atoms, will be extensively discussed in the next section.

Figure 1 shows the crystallographic free diameters of the 12- and 10-ring channels, whereas Table 7 reports the dimensions of both channels, assuming a spherical shape with radius of 1.35 Å (Shannon 1976) for the framework O atoms. According to Pluth and Smith (1990), the 12-ring dimensions can be defined by the O15-O15 and O1-O6 distances; the resulting aperture is 7.30×7.16 Å (see Table 7), which is slightly smaller than the maximum value (7.6 Å) for an ideal circular 12-ring. Regarding the 10-ring channel, following Pluth and Smith (1990), we can define its cross-section as the O8-O8 distance and the average of O9-O9 and O4-O4 distances; dimensions of 5.16×5.14 Å are obtained, which is remarkably smaller than the 5.9 Å diameter for an ideal circular 10-ring.

Extraframework species. Thirteen extraframework sites were located (Table 3 and Fig. 2); all show weak, broad, and ill-defined peaks at distances greater than 2.7 Å from the framework O atoms (except P&S6-O8 = 2.54 Å), suggesting that only a weak interaction exists between the aluminum-silicate framework and extraframework species. As a consequence, all attempts to locate the extraframework cations were unsuccessful. Some indication of their position was obtained by analysis

of the structure refinements at higher temperature (see below). On the whole, the structure refinement allocated 407 electrons of extraframework ions, to be compared with the 721 electrons given by the chemical analysis, i.e., only 56% of the total. This result is not surprising because, in many zeolites with strong disorder in the extraframework sites (as is the case in boggsite), the structure refinement usually gives a total number of electrons lower than the "true" one, as found for example in faujasite (Baur 1964), gottardiite (Alberti et al. 1996), and mutinaite (Vezzalini et al. 1997).

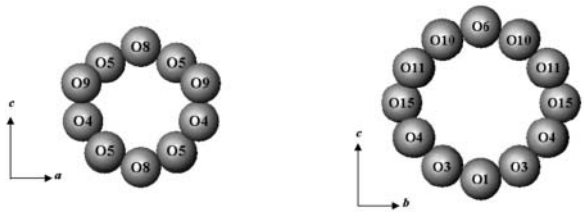

FIGURE 1. Sphere packing of O atoms defining the 10- and 12-ring channels of zeolite boggsite.

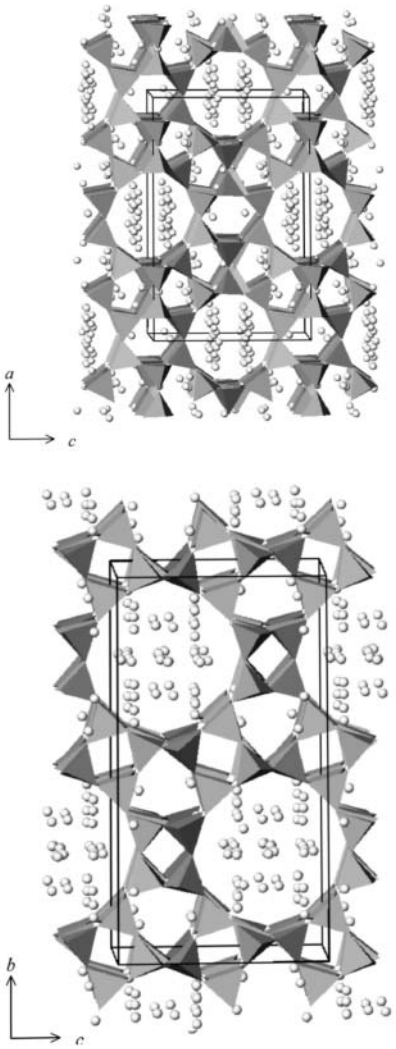

FIGURE 2. Polyhedral plot of the framework structure of boggsite at room temperature, roughly along [010] (above) and [100] (below). Extraframework species are also shown.

BOG-150 crystal structure

Framework. The dehydration process modifies the shape of the channels remarkably, influencing the O-O distances in both rings. Particularly significant are the decrease of the O9-O9 and O8-O8 distances in the 10-ring, and the increase of O15-O15 and O1-O6 in the 12-ring. This fact influences certain T-O-T angles, which change up to 10° or more (see for example T2-O15-T2 and T4-O13-T6 in Table 5). As a result, the crystallographic free area (*sensu* Baerlocher et al. 2001) of the 10-ring is strongly reduced (Δ~1.4 Å^2), whereas that of the 12-ring becomes much larger (Δ~1.5 Å^2). This behavior will be discussed in the next section.

Extraframework species. Seven extraframework sites were localized in BOG-150. Three of these were considered to host cations, the others H_2O molecules. The site with the highest occupancy (Ca1 in Table 3 and Fig. 3) was easily attributed to cations as it was present with about the same occupancy at higher temperatures, when all the H_2O molecules were lost. Ca2 was assigned as a cation site because its short coordination distances to H_2O molecules and, in particular, to the framework O atom O8 (2.27 Å) are too short for a H_2O molecule. Calcium ions at site Ca3 (see Fig. 4), as for Ca1, were located on the basis of their position being the same after complete dehydration. The other sites were attributed to H_2O on the basis of their distances from the framework O atoms and extraframework cations. With this assumption, 107 electrons were attributed to cations and 84 to H_2O molecules. Considering that the cations given by the chemical analysis account for 162 e^-, we cannot exclude the possibility

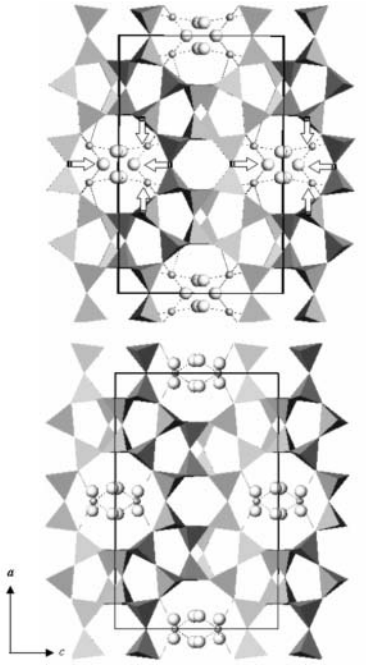

FIGURE 3. Framework structure of boggsite at 150 °C. Calcium cations (Ca1 and Ca2, above and below, respectively) are drawn as dark grey spheres and residual H_2O molecules as light grey spheres. Arrows indicate the displacement of O atoms with respect to the BOG-RT structure.

TABLE 3. Atomic coordinates, occupancy, and temperature factors for boggsite at different temperatures

Atoms	*x*	*y*	*z*	Occ.	U_{eq} or U_{iso}*	U_{11}	U_{22}	U_{33}	U_{23}	U_{13}	U_{12}
BOG-RT											
T1	0.18888(8)	0.18535(7)	0.6719(1)	1.0	0.0252(5)	0.0267(9)	0.020(1)	0.0284(7)	−0.0020(7)	0.0024(7)	−0.0007(5)
T2	0.19034(8)	0.02428(8)	0.3298(1)	1.0	0.0276(5)	0.030(1)	0.0295(9)	0.0222(7)	−0.0014(7)	−0.0020(7)	0.0003(5)
T3	0.07700(8)	0.18526(7)	0.8355(1)	1.0	0.0250(5)	0.0264(9)	0.019(1)	0.0295(6)	0.0010(7)	0.0002(7)	0.0005(5)
T4	0.07744(8)	0.02186(7)	0.1645(1)	1.0	0.0257(5)	0.025(1)	0.0285(9)	0.0232(7)	0.0005(7)	0.0005(7)	0.0005(5)
T5	0.22159(8)	0.08334(7)	0.5383(1)	1.0	0.0257(5)	0.026(1)	0.024(1)	0.0262(7)	−0.0032(7)	0.0007(7)	−0.0005(5)
T6	0.12247(8)	0.08391(7)	0.9660(1)	1.0	0.0250(5)	0.025(1)	0.023(1)	0.0262(7)	0.0047(7)	−0.0000(7)	−0.0007(5)
O1	0.1887(3)	0.25	0.6288(5)	1.0	0.039(2)	0.062(3)	0.019(4)	0.03577	0.000(3)	0.00593	0.000(2)
O2	0.1191(2)	0.1713(2)	0.7297(4)	1.0	0.044(1)	0.044(3)	0.041(3)	0.046(2)	−0.004(2)	0.010(2)	−0.002(1)
O3	0.1962(3)	0.1456(2)	0.5686(4)	1.0	0.044(1)	0.057(3)	0.032(3)	0.041(2)	−0.006(2)	0.000(2)	0.006(1)
O4	0.1897(3)	0.0703(2)	0.4254(4)	1.0	0.048(1)	0.065(3)	0.046(3)	0.033(2)	−0.009(2)	−0.006(3)	0.001(1)
O5	0.1183(2)	0.0321(2)	0.2727(4)	1.0	0.048(1)	0.038(4)	0.067(3)	0.038(3)	−0.006(2)	−0.006(2)	−0.000(1)
O6	0.0899(3)	0.25	0.8737(5)	1.0	0.035(2)	0.042(3)	0.023(4)	0.03829	0.000(3)	−0.00304	0.000
O7	0.0	0.1755(3)	0.8034(6)	1.0	0.043(2)	0.027(4)	0.044(4)	0.055(3)	−0.010(3)	0.00000	0.000
O8	0.0	0.0258(3)	0.1946(5)	1.0	0.048(2)	0.031(5)	0.070(4)	0.041(4)	0.003(3)	0.00000	0.000
O9	0.1960(3)	0.0388(2)	0.6221(4)	1.0	0.059(2)	0.099(3)	0.037(3)	0.039(2)	0.008(3)	0.014(3)	−0.005(2)
O10	0.0986(3)	0.1457(2)	0.9338(4)	1.0	0.048(1)	0.071(3)	0.029(3)	0.042(2)	0.006(3)	−0.005(2)	0.002(1)
O11	0.0950(3)	0.0721(2)	0.0820(4)	1.0	0.052(1)	0.073(3)	0.044(3)	0.037(2)	0.009(3)	0.016(3)	−0.004(1)
O12	0.2005(2)	0.0819(3)	0.9702(6)	1.0	0.078(2)	0.025(6)	0.099(6)	0.110(4)	0.039(3)	0.000(3)	−0.002(2)
O13	0.0952(3)	0.0385(2)	0.8859(4)	1.0	0.058(2)	0.096(3)	0.032(3)	0.045(2)	−0.010(3)	−0.016(3)	−0.005(2)
O14	0.25	0.1752(3)	0.75	1.0	0.051(2)	0.049(4)	0.048(4)	0.053(2)	0.000	−0.019(4)	0.000
O15	0.25	−0.0395(3)	0.75	1.0	0.054(2)	0.046(5)	0.071(4)	0.043(2)	0.000	−0.005(3)	0.000
P&S–1	0.0	0.179(1)	0.108(3)	0.48(2)	0.144(9)*						
P&S–2	0.190(1)	0.162(1)	0.207(2)	0.42(2)	0.101(7)*						
P&S–3	0.194(1)	0.25	0.045(2)	0.47(2)	0.110(9)*						
P&S–4	0.110(1)	0.165(1)	0.403(2)	0.38(2)	0.131(9)*						
P&S–5	0.0	0.164(1)	0.592(3)	0.36(2)	0.113(11)*						
P&S–6	0.0	0.030(2)	0.410(3)	0.42(2)	0.137(12)*						
P&S–7	0.071(1)	0.124(1)	0.402(2)	0.36(2)	0.109(7)*						
P&S–8	0.050(1)	0.076(1)	0.619(2)	0.40(2)	0.140(9)*						
P&S–9	0.153(2)	0.25	0.235(2)	0.32(2)	0.057(6)*						
P&S–10	0.130(2)	0.25	0.082(3)	0.37(2)	0.144(12)*						
P&S–11	0.208(3)	0.25	0.405(4)	0.21(2)	0.125(15)*						
X1	0.197(2)	0.25	0.233(3)	0.37(2)	0.091(7)*						
X2	0.0	0.086(2)	0.414(4)	0.24(2)	0.103(16)*						
BOG–150											
T1	0.18772(6)	0.18509(5)	0.6730(1)	1.0	0.0348(4)	0.0373(7)	0.0278(7)	0.0392(8)	−0.0032(5)	0.0042(6)	−0.0004(5)
T2	0.18924(6)	0.02419(5)	0.3300(1)	1.0	0.0370(4)	0.0407(8)	0.0393(7)	0.0309(7)	−0.0014(5)	−0.0049(6)	0.0012(6)
T3	0.07707(6)	0.18423(5)	0.8381(1)	1.0	0.0358(4)	0.0334(7)	0.0284(7)	0.0454(8)	0.0038(5)	0.0024(6)	0.0007(5)
T4	0.07787(6)	0.02185(5)	0.1628(1)	1.0	0.0339(4)	0.0324(7)	0.0382(7)	0.0311(7)	0.0027(5)	−0.0009(5)	0.0016(5)
T5	0.21928(6)	0.08334(5)	0.5382(1)	1.0	0.0338(4)	0.0351(7)	0.0322(7)	0.0341(7)	−0.0061(5)	0.0002(5)	−0.0016(5)
T6	0.12439(6)	0.08374(5)	0.9624(1)	1.0	0.0352(4)	0.0349(7)	0.0325(7)	0.0380(7)	0.0060(6)	−0.0022(5)	−0.0021(5)
O1	0.1827(3)	0.25	0.6340(4)	1.0	0.055(1)	0.081(4)	0.032(3)	0.050(3)	0.00000	0.003(3)	0.00000
O2	0.1190(2)	0.1666(2)	0.7333(3)	1.0	0.055(1)	0.049(2)	0.052(2)	0.062(2)	−0.005(2)	0.015(2)	−0.004(2)
O3	0.1948(2)	0.1453(1)	0.5706(3)	1.0	0.060(1)	0.085(3)	0.042(2)	0.052(2)	−0.017(2)	0.000(2)	0.013(2)
O4	0.1922(2)	0.0710(1)	0.4228(3)	1.0	0.059(1)	0.080(3)	0.051(2)	0.044(2)	−0.011(2)	−0.015(2)	0.002(2)
O5	0.1170(2)	0.0315(2)	0.2726(3)	1.0	0.065(1)	0.057(2)	0.086(3)	0.052(2)	−0.011(2)	−0.016(2)	0.008(2)
O6	0.0880(3)	0.25	0.8667(4)	1.0	0.058(1)	0.075(4)	0.029(3)	0.069(4)	0.00000	0.004(3)	0.00000
O7	0.0	0.1696(2)	0.8097(5)	1.0	0.063(1)	0.033(3)	0.062(3)	0.092(4)	0.006(3)	0.00000	0.00000
O8	0.0	0.0261(2)	0.1915(5)	1.0	0.071(2)	0.030(3)	0.090(4)	0.091(4)	−0.017(3)	0.00000	0.00000
O9	0.1869(2)	0.0393(2)	0.6189(3)	1.0	0.073(1)	0.113(4)	0.051(2)	0.053(2)	0.003(2)	0.015(2)	−0.013(2)
O10	0.1020(2)	0.1467(1)	0.9367(3)	1.0	0.062(1)	0.095(3)	0.035(2)	0.054(2)	0.006(2)	−0.009(2)	0.009(2)
O11	0.0985(2)	0.0678(2)	0.0756(3)	1.0	0.071(1)	0.103(3)	0.061(2)	0.047(2)	0.017(2)	0.014(2)	−0.005(2)
O12	0.2029(2)	0.0778(2)	0.9580(4)	1.0	0.091(2)	0.040(2)	0.122(4)	0.111(4)	0.028(3)	−0.003(2)	−0.002(2)
O13	0.0925(2)	0.0427(2)	0.8759(3)	1.0	0.068(1)	0.087(3)	0.047(2)	0.068(3)	−0.014(2)	−0.004(2)	−0.010(2)
O14	0.25	0.1756(2)	0.75	1.0	0.064(1)	0.055(3)	0.055(3)	0.081(4)	0.00000	−0.021(3)	0.00000
O15	0.25	−0.0320(3)	0.75	1.0	0.073(2)	0.055(3)	0.110(4)	0.053(3)	0.00000	−0.015(3)	0.00000
Ca1	0.0717(3)	0.0787(2)	0.6767(5)	0.278(8)	0.068(2)	0.075(4)	0.048(3)	0.080(4)	0.005(2)	−0.018(3)	−0.009(2)
Ca2	0.0	0.0278(22)	0.3690(42)	0.031(3)	0.059(13)*						
Ca3	0.0	0.1453(10)	0.0865(22)	0.083(4)	0.083(7)*						
W1	0.038(1)	0.077(1)	0.639(2)	0.31(2)	0.115(7)*						
W2	0.297(2)	0.226(1)	0.493(3)	0.14(1)	0.109(12)*						
W3	0.051(1)	0.079(1)	0.483(3)	0.16 (1)	0.126(13)*						
W4	0.0	0.151(3)	0.588(7)	0.09(1)	0.123(31)*						

Note: P&S indicates the sites also found by Pluth and Smith (1990); X are the new sites found in this work. Extraframework sites occupancies were refined using the oxygen scattering curve, whereas a silicon-aluminum mixed scattering curve was used for the T sites.

that some of the sites attributed to H_2O molecules should indeed to be assigned to cations. Moreover, is also possible that, as in BOG-RT, not all ions were located in BOG-150.

BOG-350 and BOG-500 crystal structures

Framework. No modifications in the framework seem particularly relevant at first glance. However, the distortions observed in the shape of the 10- and 12-rings, in particular a further increase (Δ~1.0 Å^2) of the 12-ring free aperture (see Table 7), show that the complete loss of H_2O molecules and consequent migration of some extraframework cations leads to an increased interaction of Ca cations with the framework O atoms.

Extraframework species. At these temperatures boggsite

TABLE 3—*CONTINUED*

Atoms	*x*	*y*	*z*	Occ.	U_{eq} or U_{iso}*	U_{11}	U_{22}	U_{33}	U_{23}	U_{13}	U_{12}
					BOG-350						
T1	0.18703(7)	0.18526(6)	0.6745(1)	1.0	0.0381(4)	0.0419(8)	0.0319(8)	0.0404(8)	–0.0040(6)	0.0009(6)	0.0013(6)
T2	0.18929(7)	0.02486(6)	0.3301(1)	1.0	0.0413(4)	0.0460(9)	0.0458(9)	0.0319(8)	–0.0033(6)	–0.0037(6)	0.0025(6)
T3	0.07692(7)	0.18450(6)	0.8410(1)	1.0	0.0412(4)	0.0367(8)	0.0322(8)	0.0547(9)	0.0066(6)	0.0046(6)	0.0020(6)
T4	0.07832(7)	0.02062(6)	0.1630(1)	1.0	0.0391(4)	0.0339(8)	0.0463(9)	0.0368(8)	0.0008(6)	–0.0000(6)	0.0000(6)
T5	0.21870(7)	0.08387(6)	0.5390(1)	1.0	0.0407(4)	0.0439(8)	0.0396(8)	0.0383(8)	–0.0079(6)	0.0002(6)	–0.0030(6)
T6	0.12429(8)	0.08451(6)	0.9639(1)	1.0	0.0443(5)	0.0462(8)	0.0404(9)	0.0460(9)	0.0075(7)	–0.0042(7)	–0.0038(7)
O1	0.1823(3)	0.25	0.6386(4)	1.0	0.058(2)	0.082(4)	0.034(3)	0.056(3)	0.00000	0.002(3)	0.00000
O2	0.1200(2)	0.1655(2)	0.7383(3)	1.0	0.063(1)	0.061(3)	0.058(3)	0.070(3)	–0.004(2)	0.019(2)	–0.006(2)
O3	0.1922(2)	0.1439(2)	0.5741(3)	1.0	0.066(1)	0.087(3)	0.052(3)	0.057(3)	–0.020(2)	–0.000(2)	0.011(2)
O4	0.1916(2)	0.0690(2)	0.4263(3)	1.0	0.067(1)	0.088(3)	0.061(3)	0.050(2)	–0.017(2)	–0.014(2)	0.002(2)
O5	0.1176(2)	0.0301(2)	0.2715(3)	1.0	0.072(1)	0.060(3)	0.098(3)	0.057(3)	–0.008(2)	–0.017(2)	0.007(2)
O6	0.0873(3)	0.25	0.8671(5)	1.0	0.066(2)	0.081(4)	0.034(3)	0.083(4)	0.00000	0.002(4)	0.00000
O7	0.0	0.1689(3)	0.8104(5)	1.0	0.068(2)	0.032(3)	0.076(5)	0.094(5)	–0.000(4)	0.00000	0.00000
O8	0.0	0.0221(3)	0.1882(6)	1.0	0.085(2)	0.039(3)	0.114(5)	0.100(5)	–0.021(4)	0.00000	0.00000
O9	0.1902(3)	0.0398(2)	0.6243(4)	1.0	0.087(2)	0.142(5)	0.057(3)	0.060(3)	0.009(2)	0.014(3)	–0.019(3)
O10	0.1007(3)	0.1465(2)	0.9392(4)	1.0	0.071(1)	0.104(4)	0.042(3)	0.064(3)	0.011(2)	–0.007(3)	0.004(2)
O11	0.0987(3)	0.0650(2)	0.0743(3)	1.0	0.078(1)	0.105(4)	0.071(3)	0.056(3)	0.024(2)	0.015(3)	–0.004(3)
O12	0.2030(2)	0.0806(3)	0.9588(5)	1.0	0.106(2)	0.041(3)	0.148(5)	0.128(5)	0.036(4)	–0.011(3)	–0.004(3)
O13	0.0950(3)	0.0439(2)	0.8735(4)	1.0	0.078(1)	0.104(4)	0.055(3)	0.073(3)	–0.014(2)	–0.004(3)	–0.020(3)
O14	0.25	0.1745(3)	0.75	1.0	0.071(2)	0.061(4)	0.074(4)	0.077(4)	0.00000	–0.027(3)	0.00000
O15	0.25	–0.0339(3)	0.75	1.0	0.079(2)	0.059(4)	0.120(5)	0.056(4)	0.00000	–0.019(3)	0.00000
Ca1	0.0785(3)	0.0797(2)	0.6956(4)	0.284(4)	0.084(2)	0.124(5)	0.055(3)	0.072(3)	0.003(2)	–0.020(3)	–0.012(3)
Ca2	0.0	0.0859(9)	0.7456(19)	0.135(5)	0.115(6)*						
Ca3	0.0	0.1388(30)	0.0729(57)	0.028(4)	0.070(15)*						
Ca3b	0.0	0.0862(31)	–0.0469(61)	0.022(4)	0.062(14)*						
Ca4	0.1944(6)	0.0807(5)	0.7831(11)	0.109(3)	0.069(3)*						
					BOG–500						
T1	0.18720(6)	0.18501(5)	0.6746(1)	1.0	0.0427(4)	0.0475(8)	0.0363(7)	0.0441(7)	–0.0054(5)	0.0012(6)	0.0009(6)
T2	0.18952(7)	0.02465(6)	0.3305(1)	1.0	0.04557(4)	0.0487(8)	0.0519(9)	0.0359(7)	–0.0027(6)	–0.0051(6)	0.0024(6)
T3	0.07665(7)	0.18452(5)	0.8404(1)	1.0	0.0463(4)	0.0405(7)	0.0371(8)	0.0613(9)	0.0073(6)	0.0061(7)	0.0023(6)
T4	0.07831(6)	0.01987(6)	0.1633(1)	1.0	0.0442(4)	0.0380(7)	0.0533(9)	0.0410(7)	0.0013(6)	0.0009(6)	–0.0003(6)
T5	0.21889(7)	0.08420(5)	0.5376(1)	1.0	0.0448(4)	0.0468(7)	0.0451(8)	0.0422(7)	–0.0080(6)	0.0002(6)	–0.0024(6)
T6	0.12373(7)	0.08518(6)	0.9669(1)	1.0	0.0483(4)	0.0489(8)	0.0459(9)	0.0499(8)	0.0081(6)	–0.0044(6)	–0.0042(6)
O1	0.1841(3)	0.25	0.6405(4)	1.0	0.067(1)	0.094(4)	0.036(3)	0.069(3)	0.00000	0.004(3)	0.00000
O2	0.1208(2)	0.1660(2)	0.7388(3)	1.0	0.072(1)	0.068(2)	0.067(2)	0.080(3)	–0.007(2)	0.024(2)	–0.007(2)
O3	0.1924(2)	0.1442(1)	0.5740(3)	1.0	0.072(1)	0.095(3)	0.057(2)	0.063(2)	–0.021(2)	–0.001(2)	0.012(2)
O4	0.1905(2)	0.0685(2)	0.4266(3)	1.0	0.072(1)	0.092(3)	0.070(2)	0.053(2)	–0.021(2)	–0.014(2)	0.004(2)
O5	0.1181(2)	0.0280(2)	0.2720(3)	1.0	0.077(1)	0.064(4)	0.106(3)	0.059(2)	–0.006(2)	–0.018(2)	0.003(2)
O6	0.0868(3)	0.25	0.8666(4)	1.0	0.076(2)	0.095(4)	0.037(3)	0.094(4)	0.00000	0.004(3)	0.00000
O7	0.0	0.1687(2)	0.8087(4)	1.0	0.075(2)	0.037(3)	0.081(4)	0.104(4)	0.002(3)	0.00000	0.00000
O8	0.0	0.0194(3)	0.1903(5)	1.0	0.087(2)	0.046(3)	0.117(5)	0.098(4)	–0.006(4)	0.00000	0.00000
O9	0.1948(3)	0.0400(2)	0.6247(3)	1.0	0.100(2)	0.170(5)	0.062(3)	0.068(3)	0.010(2)	0.017(3)	–0.021(3)
O10	0.0991(2)	0.1465(1)	0.9394(3)	1.0	0.080(1)	0.113(3)	0.050(2)	0.075(3)	0.016(2)	–0.010(2)	0.006(2)
O11	0.0966(2)	0.0662(2)	0.0774(3)	1.0	0.081(1)	0.104(3)	0.077(3)	0.061(2)	0.021(2)	0.015(2)	–0.006(2)
O12	0.2027(2)	0.0829(2)	0.9641(4)	1.0	0.115(2)	0.041(2)	0.168(5)	0.133(4)	0.036(3)	–0.006(2)	–0.005(3)
O13	0.0967(2)	0.0436(2)	0.8776(3)	1.0	0.088(1)	0.122(4)	0.064(3)	0.077(3)	–0.013(2)	–0.007(3)	–0.018(2)
O14	0.25	0.1716(2)	0.75	1.0	0.079(2)	0.068(4)	0.084(4)	0.084(4)	0.00000	–0.033(3)	0.00000
O15	0.25	–0.0344(3)	0.75	1.0	0.088(2)	0.064(4)	0.135(5)	0.064(4)	0.00000	–0.020(3)	0.00000
Ca1	0.0772(7)	0.0803(2)	0.7043(5)	0.243(5)	0.098(3)	0.147(7)	0.063(4)	0.084(4)	0.003(3)	–0.036(4)	–0.010(3)
Ca2	0.0	0.0858(8)	0.7532(17)	0.120(4)	0.110(5)*						
Ca3	0.0	0.1267(29)	0.0550(54)	0.023(3)	0.066(15)*						
Ca4	0.1929(4)	0.0789(3)	0.7779(6)	0.166(3)	0.074(2)*						

is fully dehydrated. Five cation sites were located at 350 °C; among these, Ca1 and Ca3 correspond to the same sites found at 150 °C (Figs. 5 and 6). However, whereas the occupancy of Ca1 remains almost unchanged, that of Ca3 strongly decreases; this could be interpreted as due to the alternate presence of H_2O and cations at this site at 150 °C or, more probably, to the migration of some cations to a new position. The new Ca2 site is now quite far from Ca2 at 150 °C (about 2 Å). The shift of this site is probably due to the loss of coordinating H_2O molecules and to the consequent migration to a position offering a better coordination with the framework O atoms. The two new sites, Ca3b and Ca4 (see Fig. 6), are located near the window, which joins the 10- and 12-rings and inside the cage facing the 12-ring channel [cage $5^4 6^2$ **eun** according to Pluth and Smith (1990)], respectively. The refinement at 500 °C shows that site Ca3b is empty, probably as a consequence of the migration of cations in this site to the Ca4 position; this result is supported by the increased occupancy of the latter site.

BOG-150-R and BOG-RT-R crystal structures

Framework. A comparison between the frameworks of BOG-150 and BOG-150-R, as well as BOG-RT and BOG-RT-R, indicates an almost complete restoration of the structure during the rehydration process. The only significant difference is in the O4-O11 distance of the 12-ring. In fact, this distance is 0.06 Å longer in BOG-150-R than in BOG-150 (see Table 7). This discrepancy arises from the difference in the *b* parameter, which is ~0.06 Å larger in BOG-150-R than in BOG-150. We note that all the T-O distances in the framework, as well as the atomic displacement parameters of the atoms, strongly resemble those found at the corresponding temperature steps in the dehydration process.

TABLE 3—*CONTINUED*

Atoms	*x*	*y*	*z*	Occ.	U_{eq} or U_{iso}*	U_{11}	U_{22}	U_{33}	U_{23}	U_{13}	U_{12}
					BOG-150-R						
T1	0.18746(6)	0.18525(5)	0.6732(1)	1.0	0.0350(4)	0.0373(7)	0.0286(7)	0.0390(7)	−0.0033(5)	0.0040(6)	0.0004(5)
T2	0.18913(6)	0.02434(6)	0.3300(1)	1.0	0.0375(4)	0.0420(8)	0.0394(8)	0.0308(7)	−0.0018(6)	−0.0062(6)	0.0016(6)
T3	0.07719(7)	0.18446(5)	0.8389(1)	1.0	0.0357(4)	0.0326(7)	0.0277(7)	0.0466(8)	0.0037(5)	0.0018(6)	0.0021(5)
T4	0.07795(6)	0.02185(5)	0.1630(1)	1.0	0.0340(4)	0.0314(7)	0.0380(8)	0.0324(7)	0.0022(5)	−0.0002(5)	0.0011(5)
T5	0.21920(6)	0.08338(5)	0.5392(1)	1.0	0.0351(4)	0.0358(7)	0.0341(7)	0.0351(7)	−0.0065(6)	0.0004(6)	−0.0020(5)
T6	0.12437(6)	0.08371(6)	0.9614(1)	1.0	0.0363(4)	0.0371(7)	0.0330(8)	0.0386(8)	0.0065(6)	−0.0022(6)	−0.0021(5)
O1	0.1822(3)	0.25	0.6347(4)	1.0	0.053(1)	0.079(4)	0.028(3)	0.050(3)	0.00000	0.004(3)	0.00000
O2	0.1191(2)	0.1664(2)	0.7341(3)	1.0	0.054(1)	0.047(2)	0.053(2)	0.059(2)	−0.006(2)	0.012(2)	−0.004(2)
O3	0.1942(2)	0.1448(1)	0.5714(3)	1.0	0.061(1)	0.085(3)	0.042(2)	0.054(2)	−0.017(2)	−0.001(2)	0.014(2)
O4	0.1927(2)	0.0704(2)	0.4237(3)	1.0	0.060(1)	0.083(3)	0.052(2)	0.043(2)	−0.014(2)	−0.017(2)	0.001(2)
O5	0.1165(2)	0.0316(2)	0.2729(3)	1.0	0.065(1)	0.061(3)	0.084(3)	0.050(3)	−0.009(2)	−0.016(2)	0.012(2)
O6	0.0885(3)	0.25	0.8668(4)	1.0	0.058(1)	0.077(4)	0.029(3)	0.065(4)	0.00000	0.002(3)	0.00000
O7	0.0	0.1702(2)	0.8095(5)	1.0	0.061(2)	0.027(3)	0.069(4)	0.087(4)	0.012(3)	0.00000	0.00000
O8	0.0	0.0265(3)	0.1906(5)	1.0	0.072(2)	0.034(3)	0.088(4)	0.093(4)	−0.022(4)	0.00000	0.00000
O9	0.1863(2)	0.0395(2)	0.6210(3)	1.0	0.075(1)	0.116(4)	0.050(2)	0.057(3)	0.004(2)	0.017(2)	−0.014(2)
O10	0.1019(2)	0.1463(1)	0.9374(3)	1.0	0.060(1)	0.089(3)	0.034(2)	0.055(2)	0.007(2)	−0.009(2)	0.005(2)
O11	0.0995(2)	0.0667(2)	0.0749(3)	1.0	0.071(1)	0.103(3)	0.061(3)	0.047(2)	0.017(2)	0.016(2)	−0.006(2)
O12	0.2026(2)	0.0782(2)	0.9558(5)	1.0	0.092(2)	0.038(2)	0.118(4)	0.117(4)	0.025(3)	−0.001(2)	−0.001(2)
O13	0.0925(2)	0.0430(2)	0.8741(3)	1.0	0.068(1)	0.088(3)	0.046(2)	0.068(3)	−0.012(2)	−0.005(2)	−0.010(2)
O14	0.25	0.1761(2)	0.75	1.0	0.062(1)	0.051(3)	0.055(3)	0.080(4)	0.00000	−0.016(3)	0.00000
O15	0.25	−0.0328(3)	0.75	1.0	0.073(2)	0.056(4)	0.107(4)	0.054(3)	0.00000	−0.010(3)	0.00000
Ca1	0.0727(3)	0.0791(2)	0.6767(4)	0.289(4)	0.071(1)	0.080(3)	0.045(2)	0.086(4)	0.008(2)	−0.013(3)	−0.006(2)
Ca2	0.0	0.0161(26)	0.3770(54)	0.034(4)	0.085(17)*						
Ca3	0.0	0.142(1)	0.087(3)	0.063(4)	0.081(9)*						
W1	0.039(1)	0.078(1)	0.644(2)	0.38(1)	0.134(8)*						
W2	0.301(1)	0.218(1)	0.514(2)	0.12(1)	0.097(8)*						
W3	0.050(2)	0.078(1)	0.491(3)	0.19(1)	0.127(11)*						
W4	0.0	0.138(7)	0.589(15)	0.06(1)	0.101(32)*						
					BOG–RT–R						
T1	0.18883(9)	0.18540(8)	0.6721(2)	1.0	0.0257(6)	0.028(1)	0.022(1)	0.026(1)	−0.0022(8)	0.0011(8)	−0.0004(8)
T2	0.19043(9)	0.02428(9)	0.3300(1)	1.0	0.0258(6)	0.031(1)	0.030(1)	0.020(1)	−0.0009(8)	−0.0016(8)	0.0003(8)
T3	0.07696(9)	0.18537(7)	0.8355(2)	1.0	0.0255(6)	0.027(1)	0.019(1)	0.029(1)	0.0013(7)	−0.0000(8)	0.0006(8)
T4	0.07748(9)	0.02163(8)	0.1648(1)	1.0	0.0262(6)	0.026(1)	0.030(1)	0.021(1)	0.0010(7)	0.0007(8)	0.0002(8)
T5	0.2219(1)	0.08343(8)	0.5383(2)	1.0	0.0271(6)	0.028(1)	0.027(1)	0.025(1)	−0.0036(8)	0.0007(8)	−0.0011(8)
T6	0.1221(1)	0.08402(8)	0.9664(2)	1.0	0.0272(6)	0.029(1)	0.024(1)	0.027(1)	0.0046(8)	−0.0001(8)	−0.0006(8)
O1	0.1881(4)	0.25	0.6282(6)	1.0	0.039(2)	0.060(5)	0.025(4)	0.033(7)	0.00000	0.004(2)	0.00000
O2	0.1190(3)	0.1709(2)	0.7304(4)	1.0	0.045(1)	0.046(3)	0.041(3)	0.046(3)	−0.005(3)	0.013(3)	−0.004(3)
O3	0.1957(3)	0.1454(2)	0.5687(4)	1.0	0.043(1)	0.060(7)	0.032(3)	0.035(3)	−0.005(2)	0.002(3)	0.005(2)
O4	0.1896(3)	0.0700(2)	0.4260(4)	1.0	0.047(1)	0.061(7)	0.045(3)	0.034(3)	−0.009(2)	−0.008(3)	0.003(3)
O5	0.1184(3)	0.0316(3)	0.2731(4)	1.0	0.049(2)	0.036(6)	0.070(7)	0.038(3)	−0.007(3)	−0.009(2)	0.000(3)
O6	0.0899(4)	0.25	0.8736(6)	1.0	0.036(2)	0.043(7)	0.024(7)	0.039(7)	0.00000	−0.005(3)	0.00000
O7	0.0	0.1755(3)	0.8031(6)	1.0	0.043(2)	0.025(7)	0.043(5)	0.061(5)	−0.011(7)	0.00000	0.00000
O8	0.0	0.0254(4)	0.1961(6)	1.0	0.048(2)	0.027(7)	0.075(6)	0.041(7)	0.003(7)	0.00000	0.00000
O9	0.1973(4)	0.0390(3)	0.6230(4)	1.0	0.060(2)	0.102(5)	0.038(3)	0.039(3)	0.007(3)	0.012(3)	−0.006(3)
O10	0.0980(3)	0.1458(2)	0.9342(5)	1.0	0.049(2)	0.073(7)	0.030(3)	0.041(3)	0.007(3)	−0.007(3)	0.006(3)
O11	0.0944(3)	0.0721(2)	0.0828(4)	1.0	0.052(2)	0.073(7)	0.043(3)	0.037(3)	0.007(3)	0.016(3)	−0.003(3)
O12	0.2002(3)	0.0826(4)	0.9715(7)	1.0	0.082(3)	0.027(7)	0.108(7)	0.109(7)	0.040(5)	0.002(3)	−0.000(3)
O13	0.0961(4)	0.0386(2)	0.8859(4)	1.0	0.058(2)	0.093(5)	0.032(3)	0.048(7)	−0.010(3)	−0.011(3)	−0.006(3)
O14	0.25	0.1758(3)	0.75	1.0	0.052(2)	0.046(5)	0.055(5)	0.053(5)	0.00000	−0.020(7)	0.00000
O15	0.25	−0.0401(4)	0.75	1.0	0.055(2)	0.046(5)	0.072(6)	0.045(5)	0.00000	−0.010(7)	0.00000
P&S–1	0.0	0.179(2)	0.116(3)	0.35(1)	0.128(11)*						
P&S–2	0.191(1)	0.162(1)	0.209(3)	0.29(2)	0. 108(11)*						
P&S–3	0.191(2)	0.25	0.045(3)	0.34(1)	0.105(11)*						
P&S–4	0.103(2)	0.158(1)	0.406(2)	0.26(1)	0.105(10)*						
P&S–5	0.0	0.172(2)	0.578(3)	0.28(1)	0.100(12)*						
P&S–6	0.0	0.032(1)	0.403(2)	0.336(9)	0.104(7)*						
P&S–7	0.069(1)	0.123(1)	0.400(1)	0.35(2)	0.098(7)*						
P&S–8	0.055(1)	0.0781(8)	0.618(2)	0.34(2)	0.102(8)*						
P&S–9	0.155(1)	0.25	0.123(2)	0.386(9)	0.058(6)*						
P&S–10	0.125(2)	0.25	0.108(4)	0.27(1)	0.121(12)*						
P&S–11	0.194(2)	0.25	0.140(4)	0.22(1)	0.143(22)*						
X1	0.200(2)	0.25	0.122(2)	0.28 (9)	0.089(9)*						
X2	0.0	0.103(2)	0.395(5)	0.24(1)	0.104(14)*						

Extraframework species. It is worth noting the excellent agreement between the coordinates and occupancies of the extraframework species in BOG-150 and BOG-150-R, as well as BOG-RT and BOG-RT-R, indicating an almost perfect reversibility of the dehydration-rehydration process, at least up to 500 °C.

DISCUSSION

Analysis of the unit-cell parameters reported in Table 1 shows that the volume of boggsite decreases remarkably during the dehydration process (~1%), and is partly restored (~0.4%) by the temperature increases. The later result is due to the enlarged *b*

TABLE 4. T-O distances (Å) for boggsite at different temperatures

	BOG-RT	BOG-150	BOG-350	BOG-500	BOG-150-R	BOG-RT-R
T1 –O1	1.637(3)	1.624(2)	1.614(2)	1.610(2)	1.621(2)	1.639(3)
O2	1.632(5)	1.642(3)	1.643(4)	1.631(4)	1.642(3)	1.639(5)
O3	1.635(5)	1.623(4)	1.626(4)	1.623(3)	1.626(4)	1.638(5)
O14	1.612(2)	1.609(1)	1.613(2)	1.621(2)	1.610(1)	1.609(2)
Average	1.629	1.625	1.624	1.621	1.625	1.631
T2 –O4	1.645(2)	1.630(4)	1.624(4)	1.619(3)	1.626(4)	1.644(6)
O5	1.646(5)	1.637(4)	1.627(4)	1.619(4)	1.640(4)	1.643(5)
O9	1.631(5)	1.644(4)	1.650(5)	1.648(4)	1.647(4)	1.630(6)
O15	1.625(2)	1.605(1)	1.609(2)	1.611(2)	1.607(2)	1.628(3)
Average	1.637	1.629	1.628	1.624	1.630	1.636
T3 –O2	1.636(5)	1.640(4)	1.641(4)	1.639(4)	1.641(4)	1.630(5)
O6	1.640(3)	1.619(2)	1.611(2)	1.608(2)	1.616(2)	1.637(3)
O7	1.633(3)	1.629(2)	1.635(3)	1.633(2)	1.631(2)	1.633(3)
O10	1.630(5)	1.627(4)	1.626(4)	1.626(4)	1.631(4)	1.633(5)
Average	1.635	1.629	1.628	1.627	1.630	1.633
T4 –O5	1.633(5)	1.628(4)	1.617(4)	1.622(4)	1.624(4)	1.633(5)
O8	1.621(2)	1.611(2)	1.604(2)	1.607(2)	1.609(2)	1.625(3)
O11	1.637(5)	1.618(4)	1.604(4)	1.604(4)	1.611(4)	1.633(5)
O13	1.618(5)	1.637(4)	1.642(4)	1.643(4)	1.641(4)	1.621(5)
Average	1.627	1.624	1.617	1.619	1.621	1.628
T5 –O3	1.617(5)	1.606(3)	1.593(4)	1.594(3)	1.600(3)	1.617(5)
O4	1.614(5)	1.603(4)	1.587(4)	1.582(3)	1.603(4)	1.612(6)
O9	1.597(5)	1.608(4)	1.622(4)	1.612(4)	1.618(4)	1.597(6)
O12	1.586(5)	1.570(4)	1.573(4)	1.572(4)	1.577(4)	1.584(6)
Average	1.604	1.597	1.594	1.590	1.600	1.603
T6 –O10	1.606(5)	1.595(3)	1.584(4)	1.581(3)	1.589(3)	1.607(5)
O11	1.611(5)	1.586(4)	1.584(4)	1.588(4)	1.589(4)	1.618(6)
O12	1.584(5)	1.585(4)	1.582(5)	1.583(4)	1.579(4)	1.587(6)
O13	1.591(5)	1.610(4)	1.623(4)	1.610(4)	1.613(4)	1.586(6)
Average	1.598	1.594	1.593	1.591	1.593	1.600
Overall average	1.622	1.616	1.614	1.612	1.617	1.622

TABLE 5. Boggsite framework angles (°) at different temperature

Angle	BOG-RT	BOG-150	BOG-350	BOG-500	BOG-150-R	BOG-RT-R
T1-O1-T1	140.6(5)	143.3(4)	146.0(4)	148.1(4)	143.8(4)	140.0(5)
T1-O2-T3	141.9(3)	138.6(2)	138.8(3)	140.3(3)	138.2(2)	141.6(4)
T1-O3_T5	139.1(4)	140.2(3)	142.3(3)	142.4(3)	140.7(3)	139.0(4)
T2-O4-T5	142.4(4)	144.2(2)	148.1(3)	147.8(3)	145.7(3)	142.6(4)
T2-O5-T4	144.3(4)	143.3(3)	144.9(3)	146.1(3)	142.7(3)	144.4(4)
T3-O6-T3	140.5(4)	149.4(4)	151.6(5)	151.7(4)	149.7(4)	140.5(5)
T3-O7-T3	146.4(5)	144.0(4)	141.3(4)	140.3(4)	143.8(4)	146.1(5)
T4-O8-T4	151.7(5)	152.6(4)	156.6(5)	155.1(4)	153.4(4)	150.8(5)
T2-O9-T5	152.9(4)	147.2(3)	148.1(4)	150.8(3)	145.9(3)	153.1(4)
T3-O10-T6	144.0(4)	139.6(3)	139.7(3)	140.9(3)	139.4(3)	143.9(4)
T4-O11-T6	142.9(4)	151.2(3)	155.8(3)	153.1(3)	153.3(3)	142.6(4)
T6-O12-T5	172.9(5)	169.5(4)	172.9(5)	176.9(4)	169.6(4)	172.8(6)
T4-013-T6	160.1(4)	148.0(3)	146.9(3)	150.4(3)	146.8(3)	160.6(4)
T1-O14-T1	162.7(5)	164.1(4)	161.6(4)	157.3(4)	164.5(4)	163.6(6)
T2-O15-T2	154.2(6)	166.8(4)	164.6(5)	163.5(4)	165.7(4)	153.2(6)

and *c* parameters. This finding is in agreement with the behavior of the unit-cell parameters obtained by a temperature-resolved synchrotron powder diffraction in situ study (work in progress). It is important to point out that the values of the unit-cell parameters of the in situ powder diffraction analysis clearly indicate that the structure of boggsite does not collapse up to 800 °C.

Si/Al distribution

Table 3 reports the equivalent atomic displacement parameters of the framework atoms at the different steps of the dehydration-rehydration process. They are anomalously high even at room temperature.

In fact, the average U_{eq} values of T and O atoms are 0.026 and 0.050, respectively, whereas the values usually reported for ordered zeolites are about 0.007 and 0.012, respectively. As a consequence, the T-O bond lengths appear shorter than those utilized for the Alberti and Gottardi method (1988), in which the T-O distances were obtained from structures with the lowest atomic displacement parameters. As a result the overall Al content is underestimated (see Table 8). This underestimation can be roughly evaluated by means of the rigid-body model following the approximation of Cruickshank (1956) $\Delta d(T\text{-}O) = U_{eq}(O)/2d(T\text{-}O)$, where: $\Delta d(T\text{-}O)$ is the apparent shortening of the T-O distance, and $U_{eq}(O)$ is the time-averaged mean square displacement of the O atom from its mean position. According to this approximation, the T-O distances must increase by about 0.004 Å for $U_{eq}(O) \approx 0.012$ and about 0.015 Å for $U_{eq}(O) \approx 0.050$ (at room temperature); consequently, the T-O distances found in

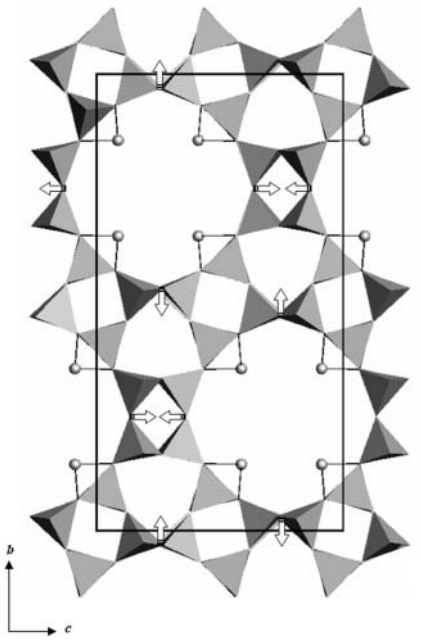

FIGURE 4. Cation position Ca3 at 150 °C, coordinated only by framework O atoms, inside the 12-ring channel of boggsite running in the [100] direction. The arrows indicate the displacement of O atoms with respect to the BOG-RT structure.

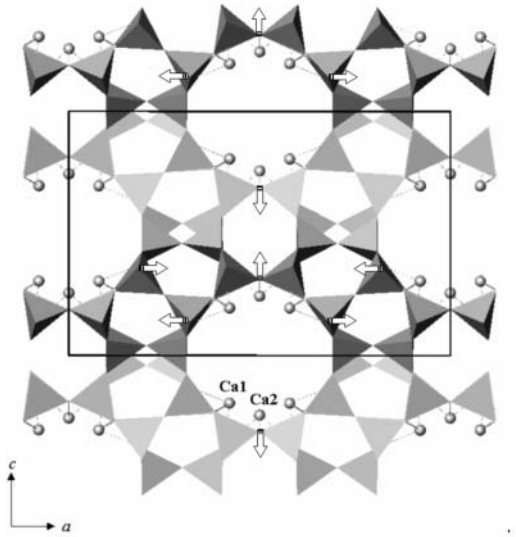

FIGURE 5. Calcium cation sites in the 10-ring channel of boggsite at 350 °C. Arrows indicate the displacement of O atoms with respect to the BOG-150 structure.

TABLE 6. Selected extraframework distances (Å) in boggsite at different temperatures

BOG-150		BOG-150-R		BOG-350		BOG-500	
Ca1–O2	2.406(6)	Ca1–O2	2.389(6)	Ca1–O2	2.275(6)	Ca1–O2	2.263(6)
Ca1–O5	2.846(7)	Ca1–O5	2.853(6)	Ca1–O5	2.766(7)	Ca1–O5	2.724(7)
Ca1–O9	2.606(7)	Ca1–O9	2.568(8)	Ca1–O9	2.599(8)	Ca1–O9	2.742(9)
Ca1–O13	2.725(7)	Ca1–O13	2.695(7)	Ca1–O13	2.463(7)	Ca1–O13	2.427(7)
Ca1–W1	2.27(3)	Ca1–W1	2.28(2)				
Ca1–W3	2.52(4)	Ca1–W3	2.42(4)	Ca2–O7	2.15(2)	Ca2–O7	2.10(2)
Ca1–W4	2.51(7)	Ca1–W4	2.31(13)	Ca2–O8	2.71(2)	Ca2–O8	2.61(2)
				Ca2–O13 ×2	2.71(2)	Ca2–O13 ×2	2.71(2)
Ca2–O5 ×2	2.66(3)	Ca2–O5 ×2	2.72(4)				
Ca2–O8	2.27(6)	Ca2–O8	2.40(7)	Ca3–O10 ×2	2.66(5)	Ca3–O10 ×2	2.53(4)
Ca2–W1 ×2	2.61(5)	Ca2–W1 ×2	2.38(6)	Ca3–O11 ×2	2.65(5)	Ca3–O11 ×2	2.43(4)
Ca2–W3 ×2	2.16(6)	Ca2–W3 ×2	2.31(7)				
						Ca4–O2	2.579(8)
Ca3–O10 ×2	2.81(2)	Ca3–O10 ×2	2.81(3)	Ca3b–O7	2.79(8)	Ca4–O9	2.179(9)
Ca3–O11 ×2	2.71(2)	Ca3–O11 ×2	2.69(2)	Ca3b–O10×2	2.37(5)	Ca4–O9	2.737(9)
				Ca3b–O11	2.57(5)	Ca4–O12	2.405(9)
				Ca3b–O13×2	2.49(4)	Ca4–O13	2.463(8)
						Ca4–O14	2.513(8)
				Ca4–O2	2.58(1)		
				Ca4–O9	2.26(1)		
				Ca4–O9	2.78(1)		
				Ca4–O12	2.26(2)		
				Ca4–O13	2.47(1)		
				Ca4–O14	2.53(1)		

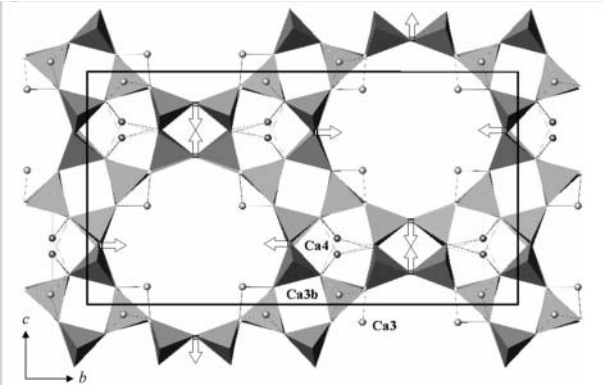

FIGURE 6. Migration of Ca cations at 350 °C from the large 12-ring channel to the small $5^4 6^2$ cage [**eun** cage according to Pluth and Smith (1990)]. Arrows indicate the displacement of O atoms with respect to the BOG-150 structure.

the refinement of boggsite are underestimated by about 0.011 Å with respect to the values used in the Alberti and Gottardi (1988) method. This value accounts for about 7% of the Al, thus justifying the underestimation of the method. If we use Cruickshank's approximation (1956) for the U_{eq}(O) at the different temperatures, the increase in T-O distances results in an increase in the Al content; the averaged value is in good agreement with the chemical analysis (see Table 8).

At first glance, the range of average T-O distances for the six independent tetrahedral sites suggests a partial ordering of the Si/Al distribution, with Al concentrated in the T1-T4 tetrahedra (see Table 4). If we now apply Cruickshank's (1956) approximation to the single tetrahedra, the increase of the Al content varies in the 6–7% range for the T1-T4 tetrahedra and about 9% for T5 and T6. Thus, partial Si/Al ordering is confirmed (see Table 9). Highly similar average T-O distances and atomic displacement parameters of the framework atoms were found by Pluth and Smith (1990) for boggsite from Goble, so that the discussion of the Si,Al distribution performed for the Mt. Adamson boggsite can be extended to the Goble sample. However, Pluth and Smith (1990) concluded that "there is no evidence for preferential occupancy of Si and Al among the six T sites," based on the evidence that adjusting T-O distances according to the riding motion model strongly reduces the differences in average T-O distances for the six tetrahedra. As a matter of fact, if we determine the overall Al content using the T-O distances corrected for the riding motion model, boggsite from both localities show about 32% Al, largely overestimated compared to the 18% given by the chemical analyses. It is therefore evident that the results of the correction for riding motion must be taken with caution.

Channel system

At first glance, an analysis of the framework coordinates suggests that very small modifications occur during the dehydration-rehydration process. On closer examination, however, this process causes remarkable modifications in both the 10- and 12-ring channel system and in the T-O-T angles; the T6-O12-T5 angle, in particular, reaches a value as high as 177° (see Table 5).

10-ring. The heating of boggsite at 150 °C causes a marked decrease of the O9-O9 distance (Δ~0.5 Å) and, to a lesser extent, of the O8-O8 distance (Δ~0.25 Å). As a result, the crystallographic free area of the ring (Table 7) decreases by more than 1 Å^2, a value about 8 Å^2 smaller than that of an ideal circular 10-ring. The decrease of the O9-O9 distance can be attributed to the Ca1-O9 bond, clearly evidenced by the remarkable increase of the T2-O9 and T5-O9 distances (see Table 4). At the same time, cation site Ca2 interacts with O8, causing it to shift in the [001] direction. Cation site Ca2 is weakly occupied, but its distance from O8 is very short (2.27 Å), so we can infer a strong interaction between Ca2 and O8. The distortion of the 10-ring is mainly reflected in the T2-O9-T5 angle, which decreases by 6° going from room temperature to 150 °C (Table 5).

When the temperature increases, the O9-O9 distance increases due to the compensation effect on O9 of the new cation site Ca4, which is strongly bonded to this O atom. At the same time, the O8-O8 distance also increases, probably as a consequence

of cation Ca2 shifting away from the framework O atom. This behavior implies a progressive increase of the free area of the ring. Note that the O5-O5 and O4-O4 distances are not much affected by the temperature (and subsequent dehydration), as these O atoms are weakly (O5) or not (O4) bonded to extraframework cations. Note that a complete reversibility of these modifications to the ring occurs during the rehydration process.

12-ring channel. The peculiarity of the behavior of the 12-ring channel lies in the increase of its free area as a consequence of the dehydration process. This behavior, unusual in zeolites (where dehydration normally causes a squashing of the channels), is due to the fact that none of the O atoms delimiting the 12-ring are involved in strong interactions with extraframework cations located toward the center of the channels.

In BOG-150 the O15-O15 distance is 0.35 Å larger than in BOG-RT (see Table 7); this result can be easily explained. In fact, together with O4, O5, and O9, O15 builds the tetrahedron T2. The O atoms O15 and O9 are not bonded to extraframework cations and, as a result, their distance from T2 suddenly decreases [Δ(T2-O15) = -0.020 Å; Δ(T2-O4) = –0.017 Å] (see Table 4). O atom O5, which is at a great distance from Ca1, does not change its bond distance significantly from T2; on the contrary, as pointed out before, O9 is strongly bonded to Ca1, as evidenced by the increase of the T2-O9 distance [Δ(T2-O9) = +0.013 Å]. At the same time, the cations at Ca1 and, to a lesser extent, Ca2 impose a rotation of tetrahedron T2; as a consequence, each of the two O15 atoms is shifted by about 0.16 Å along *b*, far from the center of the ring. As a result, by summing this shift to the decrease in the T2-O15 distance described above, we obtain an increase of the O15-O15 distance of 0.35 Å. At the same time, the T2-O15-T2 angle increases by ~13° (from ~154° to ~167°; see Table 5). If we now examine the structure of boggsite in the [010] direction, two structural units can be distinguished: the 12-ring, and a dense packing of tetrahedra formed by two $5^4 6^2$ polyhedral subunits [**eun** units according to Pluth and Smith (1990)]. As parameter *b* is about 0.1 Å shorter at 150 °C than at RT, it can be seen that, since the 12-ring is 0.35 Å larger, the dense packing is reduced by as much as 0.45 Å. We can explain the increasing O1-O6 distance (0.15 Å), which develops in the [001] direction, in a similar way. In this case we also observe a decrease in the T-O distances of these two framework O atoms [Δ(T1-O1) = –0.12 Å; Δ(T3-O6) = –0.020 Å]. This effect is due to the strong interaction of the cation at Ca1 with the O atom at O2 which bridges the tetrahedral cations T1 and T3. As a consequence, O1 and O6 shift away from the center of the 12-ring by about 0.08 Å, a value that justifies the increase of the O1-O6 distance. This shift affects the T1-O1-T1 and T3-O6-T3 angles, which widen by ~3° and ~8°, respectively.

TABLE 7. Selected distances (Å) and areas (Å²) across 10- and 12-ring channels

Sample	10 MR	C.F.A.*	O9-O9	O4-O4	O5-O5	O8-O8
Pluth and Smith (1990)	5.16 × 5.09	20.3	5.18	4.99	5.02	5.16
BOG-RT	5.16 × 5.14	20.4	5.29	4.98	4.97	5.16
BOG-150	4.92 × 4.92	19.0	4.81	5.02	4.93	4.92
BOG-350	4.96 × 4.96	19.3	4.93	4.98	4.97	4.96
BOG-500	5.03 × 5.03	19.7	5.11	4.94	4.96	5.03
BOG-150-R	4.92 × 4.92	19.0	4.79	5.04	4.92	4.92
BOG-RT-R	5.18 × 5.15	20.5	5.30	4.99	4.99	5.18
Sample	**12MR**	**C.F.A.***	**O15–O15**	**O4–O11**	**O3–O10**	**O1–O6**
Pluth and Smith (1990)	7.42 × 7.18	40.3	7.42	7.05	7.02	7.18
BOG-RT	7.30 × 7.16	40.0	7.30	7.07	7.01	7.16
BOG-150	7.65 × 7.31	41.5	7.65	7.15	6.99	7.31
BOG-350	7.60 × 7.39	42.4	7.60	7.30	7.09	7.39
BOG-500	7.57 × 7.45	42.3	7.57	7.27	7.05	7.45
BOG-150-R	7.64 × 7.32	41.8	7.64	7.21	7.00	7.32
BOG-RT-R	7.31 × 7.16	40.1	7.31	7.09	7.03	7.16

* Crystallographic Free Area [*sensu* Baerlocher et al. (2001)] calculated using for the diameter of the ring the mean of the O–O distances reported in the Table.

In BOG-350, the O15-O15 distance is about 0.05 Å shorter than in BOG-150, in spite of the 0.09 Å increase of *b* (see Table 1), while the O1-O6 distance increases by 0.08 Å. This effect is due to the new cation site Ca4. As pointed out before, Ca4 strongly interacts with O9 in opposition to the effect of Ca1. At the same time, Ca4 sums its effect to Ca1 on O atom O2, increasing the shift of O1 and, to a lesser extent, O6 in the [001] direction. This shift adds to the increase of *b* (0.09 Å), thus justifying the enlargement of the O1-O6 distance. Cations at Ca4 are also responsible for the enlargement of the O4-O11 distance (0.23 Å with respect to BOG-RT; see Table 7). This interaction is evidenced by the increase of T-O13 [Δ(T4-O13) = + 0.24 Å; Δ(T6-O13) = + 0.032 Å] and by the corresponding remarkable decrease of T-O11 and T-O4 (as reported in Table 7). As Ca4 is located inside the polyhedral subunit **eun,** it results in an enlargement of the 12-ring. The increase of the O1-O6 distance is still more evident in BOG-500; it is easy to associate the increase of this distance to the occupancy of Ca4, higher in BOG-500 with respect to BOG-350. We note that the widening of T-O-T angles of the O atoms delimiting the channel strictly follows the variations of the corresponding O-O distances.

Table 7 shows that the free area of the 12-ring increases by up to about 2 Å² as the temperature increases, reaching a value (~42.4 Å²) not very far from its ideal one (~45.5 Å²). If we consider that cation sites Ca1, Ca2, and Ca3 are near the walls of the channel (see Figs. 5 and 6) and Ca4 is outside the channel, dehydrated boggsite shows a large, empty aperture at the center of the 12-ring channel (~28 Å²). It has already been pointed out in this study that the dehydration-rehydration process in boggsite is completely reversible. This behavior is even more clearly evidenced by the reversibility of distances and angles of the channel system upon rehydration (see Tables 6 and 7).

Extraframework species. As pointed out in the "Results" section, any attempt to locate extraframework cations in BOG-RT was unsuccessful. The structure refinement of BOG-150, however, can be used to recognize some cation sites in BOG-RT. In particular, site P&S8 in BOG-RT resembles Ca1 in BOG-150, whereas sites P&S6 and P&S1 are not far from the cation posi-

TABLE 8. Al-fraction (%) in boggsite at different temperatures

	BOG-RT	BOG-150	BOG-350	BOG-500	BOG-150-R	BOG-RT-R
Al-fraction according to the method of Alberti and Gottardi (1988)	13	7	5	4	7	13
Underestimation of the Al-fraction according to the rigid-body approximation (Cruickshank 1956)	7	11	12	14	11	7
Al-fraction corrected for rigid-body approximation (Cruickshank 1956)	20	18	18	18	18	20
Average Al-fraction			18.7			

TABLE 9. Al-fraction (%) in the tetrahedra according to the method of Alberti and Gottardi (1988) and corrected for the rigid-body approximation (Cruickshank 1956)

	BOG-RT	BOG-150	BOG-350	BOG-500	BOG-150-R	BOG-RT-R	Average
T1	24	22	23	22	23	26	23
T2	33	30	31	30	31	32	31
T3	26	23	23	24	24	26	24
T4	26	23	20	23	22	26	23
T5	7	4	5	4	6	7	6
T6	5	3	4	4	1	6	4

tions Ca2 and Ca3 in BOG-150. Sites Ca1 and Ca3 remain at higher temperatures, whereas Ca2, which is weakly occupied, disappears at 350 °C. At this temperature an important new site, called Ca4, is located at the center of the **eun** subunit and displays a fairly regular 6-fold coordination with framework O atoms.

The most interesting feature of extraframework cations in BOG-350 is the coordination number of sites Ca1, Ca2, and Ca3. In fact, if we assume the value 3.0 Å as a maximum coordination distance for Ca, all these sites are 4-coordinated. A similar feature also characterizes the structure of BOG-500. The presence of such a coordination number for Ca in the boggsite structure appears quite remarkable when compared to the high-temperature, dehydrated forms of several Ca-rich zeolites, such as mesolite, scolecite, laumontite, garronite, gismondine, yugawaralite, and epistilbite (see Cruciani et al. 2003 and references therein). Temperature-resolved investigations of these zeolites have shown that increased interaction of the Ca cation with framework O atoms and, in particular, a reduction in Ca coordination below six (seven for yugawaralite) can be regarded as triggering the collapse of the structure. It is noteworthy that a similar behavior has also been reported by Merlino et al. (2001) for Ca coordinated to "zeolitic" water in a non-zeolite mineral, 11 Å "normal" tobermorite, upon heating. The structure collapse clearly does not occur in boggsite. As a matter of fact, Seryotkin et al. (2003) also reported fourfold coordination for Ca in dehydrated wairakite. The presence of fourfold Ca in the dehydrated forms of both boggsite and wairakite strongly emphasizes the importance of the framework topology category (collapsible or non-collapsible, according to Baur 1992), besides the extraframework cation type, in explaining and predicting the occurrence of a collapsed phase in dehydrated zeolite forms. Furthermore, it should be considered that the framework of wairakite is very dense, and rings larger than six are not present in the structure.

In brief, boggsite has provided an extremely rigid structure whose cell volume contraction is less than 1.4%, the lowest found to date in natural zeolites. The high-temperature structure is capable to hold Ca cations, in fourfold coordination, a feature that has been reported as leading to structure collapse. As a final remark, we point out that the strong disorder found in boggsite by Pluth and Smith (1990) and confirmed in the present work can be regarded as a distinctive feature, common in the other zeolites found in Antarctica (Alberti et al. 1996, Vezzalini et al. 1997), likely indicating an unusual environment during zeolite crystal growth (e.g., rapid cooling).

ACKNOWLEDGMENTS

The authors thank the Centro di Strutturistica Diffrattometrica of the University of Ferrara for X-ray data collection. Italian PNRA and MIUR ("Zeolites, materials of interest for industry and environment: synthesis, crystal structure, stability and applications." COFIN 2001) are acknowledged for financial support. The "Consiglio Nazionale delle Ricerche" of Italy is acknowledged for funding the electron microprobe laboratory at the Dipartimento di Scienze della Terra of the University of Modena e Reggio Emilia.

REFERENCES CITED

Alberti, A. (1979) Possible 4-connected frameworks with 4-4-1 unit found in heulandite, stilbite, brewsterite, and scolecite. American Mineralogist, 64, 1188–1198.

Alberti, A. and Gottardi, G. (1988) The determination of Al-content in the tetrahedra of framework silicates. Zeitschrift für Kristallographie, 184, 49–61.

Alberti, A., Gottardi, G., and Lai, T. (1990) The determination of (Si,Al) distribution in zeolites. In D. Bathomeuf, E.G. Deroune, and W. Hölderich, Eds., Guidelines for mastering the properties of molecular sieves. Relationship between the physicochemical properties of zeolitic systems and their low dimensionality. Series B Physics, 221, 145–155. Plenum Press New York and London.

Alberti, A., Vezzalini, G., Galli, E., and Quartieri, S. (1996) The crystal structure of gottardiite, a new natural zeolite. European Journal of Mineralogy, 8, 69–75.

Baerlocher, Ch., Meier, W.M., and Olson, D.H. (2001) Atlas of Zeolite Framework Types, 5th revised edition. Elsevier, London.

Baur, W.H. (1964) On the cation and water positions in faujasite. American Mineralogist, 49, 697–704.

——— (1992) Self-limiting distortion by antirotating hinges is the principle of flexible but noncollapsible framework. Journal of Solid State Chemistry, 97, 243–247.

Cruciani, G., Martucci, A., and Meneghini, C. (2003) Dehydration dynamics of epistilbite by in situ time resolved synchrotron powder diffraction. European Journal of Mineralogy, 15, 257–266.

Cruickshank, D.W.J. (1956) Errors in bond lengths due to rotational oscillations of molecules. Acta Crystallographica, 9, 757–758.

Galli, E., Quartieri, S., Vezzalini, G., and Alberti, A. (1995) Boggsite and tschernichite-type zeolites from Mt. Adamson, Northern Victoria land (Antarctica). European Journal of Mineralogy, 7, 1029–1032.

Howard, D.G., Tschernich, R.W., Smith, J.V., and Klein, G.L. (1990) Boggsite, a new high-silica zeolite from Goble, Columbia County, Oregon. American Mineralogist, 75, 1200–1204.

Merlino, S., Bonaccorsi, E., and Armbruster, T. (2001) The real structure of tobermorite 11 Å: normal and anomalous forms, OD character and polytypic modifications. European Journal of Mineralogy, 13, 577–590.

Otwinowski, Z. and Minor, W. (1997) Processing of X-ray Diffraction Data Collected in Oscillation Mode. In C.W. Carter Jr. and R.M. Sweet, Eds., Methods in Enzymology: Macromolecular Crystallography, Part A, p. 307–326. Academic Press, New York.

Pluth, J.J. and Smith, J.V. (1990) Crystal structure of boggsite, a new high-silica zeolite with the first three-dimensional channel system bounded by both 12- and 10-rings. American Mineralogist, 75, 501–507.

Seryotkin, Y.V., Joswig, W., Bakakin, V.V., Belitsky, I.A., and Fursenko, B.A. (2003) High-temperature crystal structure of wairakite. European Journal of Mineralogy, 15, 475–484.

Shannon, G.M. (1976) Revised effective ionic radii and systematic studies of interatomic distances in halides and chalcogenides. Acta Crystallographica, A32, 751–767.

Sheldrick, G.M. (1993) SHELXL93, Program for crystal structure determinations. University of Cambrige, Cambrige, U.K.

Smith, J.V. (2000) Microporous and other framework materials with zeolite-type structures. In W.H. Baur and R.X. Fischer, Eds., Landolt-Börnstein New Series Group IV, Volume 14, Subvolume A: Tetrahedral frameworks of zeolites, clathrates and related materials. Springer, Berlin.

Tuinstra, F. and Fraase Storm, G.M. (1978) A universal high-temperature device for single-crystal diffraction. Journal of Applied Crystallography 11, 257–259.

Vezzalini, G., Quartieri, S., Galli, E., Alberti, A., Cruciani, G., and Kvick, Å. (1997) Crystal structure of the zeolite mutinaite, the natural analog of ZSM-5. Zeolites, 19, 323.

MANUSCRIPT RECEIVED OCTOBER 9, 2003
MANUSCRIPT ACCEPTED JANUARY 22, 2004
MANUSCRIPT HANDLED BY LEE GROAT